Five Centuries of Groundwater Elevations Provide Evidence of Shifting Climate Drivers and Human Influences on Water Resources in North Central Florida

Evan R. Larson[1], Tom Mirti[2*], Thomas Wilding[1†], and Chris A. Underwood[1]

[1]Department of Environmental Sciences & Society, University of Wisconsin-Platteville

[2] Suwannee River Water Management District, Live Oak, Florida

Corresponding author: Evan Larson (larsonev@uwplatt.edu)

* Current affiliation: Retired; †Current affiliation: Nicolet Area Technical College

Key Points:

- A 517-yr reconstruction of groundwater elevation indicates recent lows in North Central Florida approached megadrought conditions
- These extreme low groundwater elevations were likely caused in part by climate drivers and amplified by groundwater extraction
- Coupled oceanic-atmospheric phenomena drive variability in the persistence of groundwater elevations in North Central Florida

Abstract

Groundwater depletion is a concern around the world with implications for food security, ecological resilience, and human conflict. Long-term perspectives provided by tree ring-based reconstructions can improve understanding of factors driving variability in groundwater elevations, but such reconstructions are rare to date. Here, we report a set of new 546-year tree-ring chronologies developed from living and remnant longleaf pine (*Pinus palustris*) trees that, when combined with existing bald cypress (*Taxodium distichum*) tree-ring chronologies, were used to create a set of nested reconstructions of mean annual groundwater elevation for North Central Florida that together explain 63% of the variance in instrumental measurements and span 1498–2015. Split calibration confirms the skill of the reconstructions, but coefficient of efficiency metrics and significant autocorrelation in the regression residuals indicate a weakening relationship between tree growth and groundwater elevation over recent decades. Comparison to data from a nearby groundwater well suggests extraction of groundwater is likely contributing to this weakening signal. Periodicity within the reconstruction and comparison with global sea surface temperatures highlight the role of El Niño-Southern Oscillation (ENSO) in driving groundwater elevations, but the strength of this role varies substantially over time. Atlantic and Pacific sea surface temperatures modulate ENSO influences, and comparisons to multiple proxy-based reconstructions indicate an inconsistent and weaker influence of ENSO prior to the 1800s. Our results highlight the dynamic influence of ocean-atmospheric phenomena on groundwater resources in North Central Florida and build on instrumental records to better depict the long-term range of groundwater elevations.

Plain Language Summary

Groundwater is an important source of freshwater for municipal and agricultural uses around the world. One major challenge to ensuring groundwater use is sustainable is that long-term records of its availability are scarce. This means we do not fully understand all the factors that influence groundwater availability or how groundwater resources may change in the future. One way to expand perspectives on groundwater resources is to use proxies, such as tree rings, to estimate past environmental conditions. Our team gathered tree-ring samples from old-growth longleaf pine trees in North Central Florida to develop a record of tree growth that spanned 546 years, from 1472–2018. Climate conditions that influenced tree growth at our site also influenced groundwater elevation. Based on this relationship, we reconstructed over five centuries of groundwater elevation changes. From this reconstruction, we now know that while deeper and more prolonged droughts than anything experienced during the instrumental record occurred in the past, the combined influences of climate and groundwater extraction drove recent groundwater elevations to lows comparable to some of the worst droughts in the past 500 years. As population continues to grow in Florida, residents and water managers can expect to face more extremes in groundwater elevations.

1 Introduction

Groundwater depletion is a significant concern in many regions of the world with critical implications for food security, ecological systems, and human conflict (Bierkens & Wada, 2019; Jasechko & Perrone, 2021). In the United States, declining groundwater levels documented across several broad areas raise concerns about the impacts of extraction and overexploitation on groundwater resources at regional scales (Jasechko & Perrone, 2021). For example, groundwater elevations in parts of the southeastern United States have declined over recent decades (Sutton et al., 2021), despite instrumental and tree-ring based perspectives indicating relatively wet conditions compared to recent decades and even centuries (Pederson et al., 2012). These contrasting patterns suggest that groundwater extraction for municipal and agricultural uses is outpacing recharge rates (e.g., de Graaf et al., 2019); however, in most cases instrumental records of groundwater are too short to clearly disentangle the effects of climate variability and extraction on groundwater elevations.

The longer-term perspectives enabled by proxy-based reconstructions would be immensely useful in considering changing groundwater conditions, but groundwater elevation is a challenging target to reconstruct. First, most time series of groundwater elevations are relatively short and many include numerous gaps from missing observations. This poses a challenge for robust calibration and verification (Fritts, 1976), particularly given the long-term persistence in groundwater systems relative to other aspects of climate such as precipitation (Sutton et al., 2021). Second, spatial variability in recharge mechanisms and the climate sensitivity of groundwater systems may differ from the available proxies, particularly trees whose growth is linked to atmospheric and surface conditions (Hunter et al., 2020). Third, widespread

groundwater extraction for agricultural and municipal purposes is altering groundwater levels around the world (Bierkens & Wada, 2019), potentially introducing trends in groundwater levels that are unrelated to atmospheric conditions that would otherwise link patterns in tree growth to changes in groundwater levels (Ferguson & St. George, 2003). Despite these challenges, the potential value of expanding perspectives on groundwater variability over multiple centuries to better understand their human and climatic drivers is immense and worth pursuing (Gholami et al., 2017), particularly where oceanic-atmospheric phenomena influence hydrologic conditions on time scales beyond the instrumental record (Gordu & Nachabe, 2021). This is the case in the southeastern United States, where growing populations are increasing demands on groundwater resources in a region where global sea surface temperatures strongly influence hydrologic conditions (Enfield et al., 2001; Schmidt et al., 2001).

Among southeastern U.S. aquifers, the Floridian Aquifer System (FAS) covers approximately 100,000 square miles and is the primary source of drinking water for millions of residents in Florida and Georgia (Miller, 1990). Well data across the FAS show increasing extraction and a decline in elevation of about 0.1–0.15 meter per year since 1950 (Barlow, 2003; Marella & Berndt, 2005). Cones of depression have formed around major cities within the FAS, such as Jacksonville, Florida, and in some cases local potentiometric gradients have reversed over instrumental records, creating the potential for encroachment of saltwater from coastal regions or from deep parts of the aquifer that contain saltwater (Miller, 1990). The installation of high-capacity wells to provide irrigation on sandy sites has also increased groundwater extraction in more rural areas (Marella & Berndt, 2005). Concerns over these groundwater impacts have been amplified by growing populations and increased demand for water. In northern Florida alone,

105 population increased by nearly 1 million residents since the early 2000s, placing considerable
106 new demand on water resources (BEBR, 2011, 2020). With a growing population in the region
107 and a diminishing groundwater supply, water resource managers in the Southeastern United
108 States could benefit from the long-term perspective on water resource variability offered by
109 dendrochronology.
110
111 Here, we report a set of new 546-year tree-ring chronologies developed from the rings of living
112 and remnant old growth longleaf pine (*Pinus palustris*) in North Central Florida that, when
113 combined with existing tree-ring chronologies developed from bald cypress (*Taxodium*
114 *distichum*), enable the first annually resolved, multi-century reconstruction of groundwater
115 elevation for the state. The resulting reconstruction extends records of groundwater by over 450
116 years, provides a long-term perspective on shifting climate influences on groundwater elevation,
117 and enables contextualization of recent declines in groundwater elevations for the region that are
118 unprecedented in the historical record.
119

120 **2 Methods and Results**

121 2.1 Study area and field methods

122 Our study area is located in Goethe State Forest (GSF), a forest reserve in close proximity to
123 three of Florida's five water management districts: the Suwannee River Water Management
124 District (SRWMD), the St. Johns River Water Management District, and the Southwest Florida
125 Water Management District (Figure 1a). These districts collectively encompass over 7.75 million
126 hectares and are responsible for water supply planning for approximately 10 million people. The

127 landscape is relatively flat with low relief. Soils are sandy and extremely well drained, with
128 subtle changes in topography creating substantial differences in plant communities. Current
129 vegetation includes open stands of longleaf and slash pine (*Pinus elliottii*) with a saw palmetto
130 (*Serenoa repens*) understory in upland settings, while relief of only 1–2 m results in marshes and
131 wetlands dominated by slash pine and bald cypress (Figure 1b, 1c). The forest is managed for
132 timber production, restoration of wire grass (*Aristida stricta*) plant communities, and red
133 cockaded woodpecker (*Picoides borealis*) habitat. Mechanical thinning between 2000–2007 and
134 widespread use of prescribed fire has been used to maintain an open savanna structure. During
135 this period of intensive management, numerous old-growth longleaf pines were identified, along
136 with an abundance of remnant stumps from logging *ca.* 1850 (Outland III, 2004).
137
138 Groundwater elevation data are available from a network of monitoring wells that generally span
139 the last several decades, however missing or discontinuous observations are common among
140 these datasets. We screened numerous well logs from across the region and included two in the
141 analyses presented here. First, the USGS Newberry well (S101722101) is the nearest long-term
142 well to Goethe State Forest, one of the longest and most complete records investigated, and
143 represents a continuous set of monthly observations from 1959–2020 (SRWMD, 2020). The
144 second well considered here is the Cross City well (S101210001) which spans 1958–2020 but is
145 more distant from the study site and includes 164 missing monthly observations, most of which
146 occur from 1963–1979 (SRWMD, 2020). The value of the Cross City well is that it is farther
147 from areas of intense groundwater use and should therefore represent past groundwater elevation
148 most strongly influenced by climatic drivers rather than land use. For both wells, we calculated

149 average annual groundwater elevation from all available observations per year. The years 1974
150 and 1975 present gaps in the Cross City well time series where no observations were taken.
151
152
153

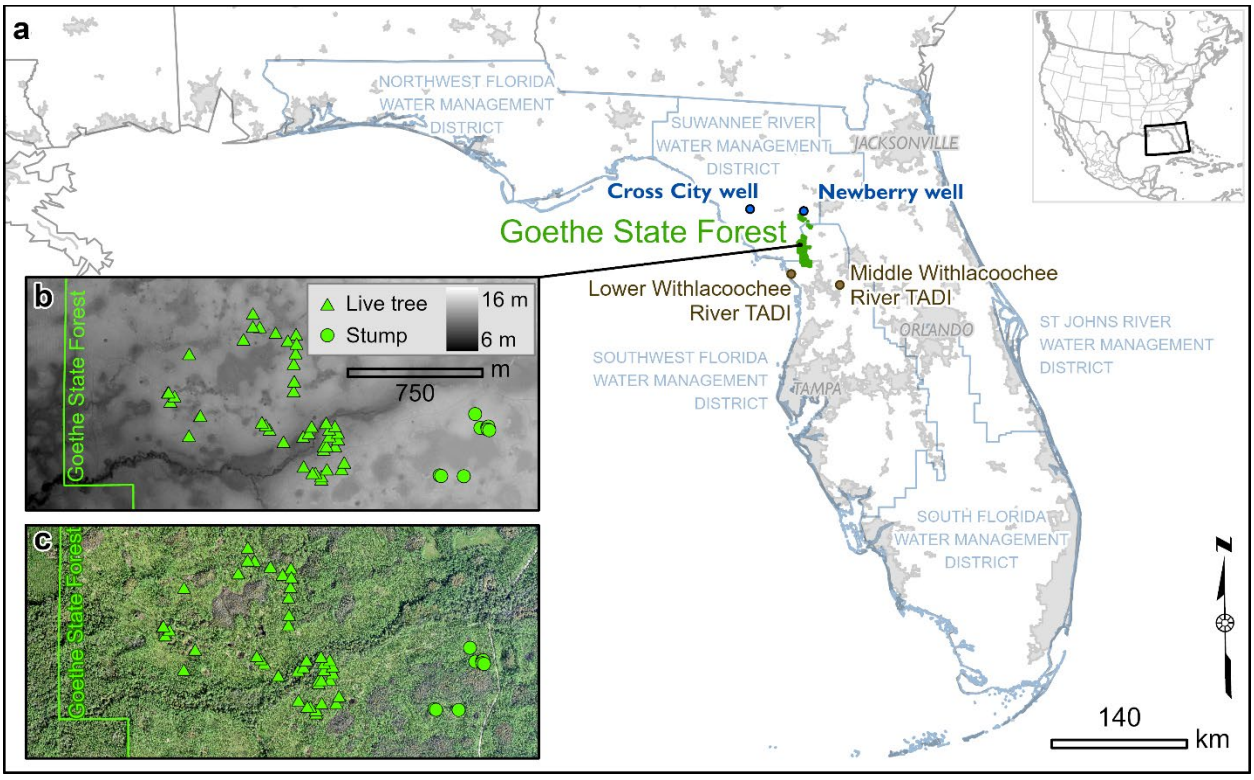

154

155 **Figure 1.** The study area in North Central Florida. (a) The location of Goethe State Forest
156 relative to the two wells used in this study, Florida water management district boundaries, and
157 major metropolitan areas, (b) a subset of the study area shown with a LiDAR-based DEM to
158 illustrate the distribution of sampled longleaf pine (*Pinus palustris*) trees and stumps relative to
159 subtle variations in topography, and (c) the same extent shown with color aerial imagery to
160 illustrate vegetation patterns created by topography.
161

Preliminary work in 2003 produced tree-ring chronologies from living old-growth longleaf pine and identified links between tree growth and hydrologic conditions in North Central Florida (Crockett et al., 2010). Additional sampling of both living trees and a small number of remnant stumps in 2008 produced a 438-yr chronology with significant climate information that provided important contributions to a reconstruction of the Suwannee River (Harley et al., 2017), but low sample depth in the mid-1800s coupled with a period of suppressed growth, both likely related to logging and resin extraction for the naval stores industry (Outland III, 2004), highlighted the need for additional sampling. A third phase of sampling in 2017 and 2019 specifically targeted living trees to update the existing chronologies and additional remnant longleaf pine stumps to extend the chronology further into the past, increase sample depth in the overlap between living trees and remnant stumps, and enhance signal strength during the 1800s.

Sampling focused on living trees that visually exhibited old-growth characteristics, including the presence of robust limbs in the canopy, flattened canopy structure, absence of lower limb stubs, acute distortion of sub-canopy limbs, and the presence of peel scars associated with turpentine production, which ended around 70 years ago in northern Florida (Figure 2a, 2b). Increment core samples were collected along 1–4 radial transects of each living tree, with the number of transects determined by the shape, size, and symmetry of the tree. Stumps were initially sampled opportunistically until their value became more evident. Later, to improve the efficacy of targeted stump sampling, the study area was scouted following winter prescribed fires that reduced ground cover and maximized the likelihood of locating low-profile stumps. Stump sampling specifically targeted specimens that exhibited deep weathering, char, and evidence of box-cuts associated with resin collection activities in the 1800s. All sampled stumps were cut

with a chainsaw as low to the ground as possible to ensure collection of the maximum number of growth rings, with later recognition that ground-level samples also enhanced the potential for their use in fire history research (Huffman & Rother, 2017). A visual chronosequence emerged, with different types of cambial scars associated with different periods of turpentine harvesting techniques and the oldest samples coming from snags that were likely from trees that died prior to 1800s logging and turpentine activities (Figure 2b, 2c, 2d).

Figure 2. Site and tree characteristics used to guide sample collection. (a) Open stand structure has been maintained through mechanical treatments and prescribed burns, with old growth longleaf pine retained to provide habitat for the endangered red cockaded woodpecker (indicated by white band on the tree at far right). Relative sample age was estimated by (b) living trees with "catface" scars associated with turpentining activities in the late 1800s and early 1900s, (c) box cuts associated with turpentine activity in the middle to late 1800s, and (d) remnant snags with no evidence of turpentine collection from trees that likely died prior to logging or the establishment of industrial turpentine activities on site.

2.2 Tree Ring Chronology Development

Cross sections were frozen at *ca.* –20 °C for at least 24 hours prior to sanding to reduce the emergence of resin during the finishing process, then surfaced using hand-held belt sanders and progressing from ANSI 40-grit to ANSI 400-grit. Pneumatic palm sanders with microfinishing film were then used to maintain cool temperatures while progressively sanding to a final grit of 20-micron sanding discs. Each sample was polished with steel wool to achieve the final surface. A similar progression of sanding was applied to core samples, but by hand-sanding.

Two to four paths were identified on each cross section, depending on the shape and condition of the sample, while a single transect was identified on each core sample. The annual rings of each sample were identified under 4.5–40× magnification and internally crossdated to account for locally-absent growth rings and intra-annual variations in wood density, commonly referred to as false rings. Each path was scanned at 1800 dpi optical resolution using an Epson 10000XL flatbed scanner. The images of each path were imported to WinDENDRO v2014 and measured for total ring width (TRW), earlywood width (EW), and latewood width (LW). The boundary between earlywood and latewood growth was determined as the first formation of latewood cells within each ring and a regression-based latewood measurement series (LW_{reg}) was created for each path by removing the shared variability between earlywood and latewood widths through linear regression (sensu Griffin et al., 2011).

Crossdating was strong within the final longleaf pine tree-ring data set, with a total of 172 dated measurement series from 91 trees, of which 59 were living and 32 were remnants. The data set spanned the years 1472–2018 and exhibited an expressed population signal of >0.85 from 1505–

2018 (Figure 3a, 3b). Visual inspection of the raw longleaf pine ring width data indicated a distinct decade or more of suppressed growth from the late 1800s to the early 1900s, likely the result of extensive cambial damage from turpentining activities, followed by growth releases (Figure 3a). We emphasized the variability likely related to interannual climate variations despite these releases and suppressions in tree growth by normalizing each ring-width measurement series using a power transformation method described by Cook and Peters (1997). The normalized measurement series were then used to develop a total of 16 versions of standardized ring width-index (RWI) chronologies from the longleaf pine, as described below.

First, two versions of standard (STD) chronologies were created for each type of measurement collected from the longleaf pine (TRW, EW, LW, and LW_{reg}). Each normalized measurement series was fit with a spline of 50% frequency cutoff at a 30-year frequency to remove low-frequency variability from the ring width series (Cook & Peters, 1981). The values from each resulting ring-width index series were then used to calculate an annually-resolved RWI chronology using a robust bi-weight mean (Cook, 1985). This resulted in chronologies with minimal evidence of the disturbance effects (GSF30; Figure 3b). Second, each normalized measurement series was fit using a stiffer spline with 50% frequency cutoff at the 100-year frequency to retain a greater proportion of the low-frequency variability within the ring-width series, and again combined into RWI chronologies using bi-weight means of annual values. The resulting chronologies retained more information that could provide insight to the low-frequency variability of hydrologic conditions in Florida, but also retained more evidence of the growth suppression (GSF100; Figure 3b). This produced eight STD chronologies, including TRW, EW, LW, and LW_{reg} based on both the GSF30 and GSF100 standardization approaches.

Second, an additional eight residual (RES) chronologies were created by applying the same standardization methods described above (GSF30 and GSF100), but fitting each of the individual ring width index series to an Autoregressive-Moving-Average Model before combining the resulting annual values using a robust bi-weight mean (Meko, 1981). The RES chronologies therefore expressed less autocorrelation and better emphasized inter-annual variations of tree growth than the STD chronologies. In all, this resulted in a total of sixteen standardized tree-ring chronologies from the longleaf pine measurements: standard (STD) and residual (RES) chronologies based on TRW, EW, LW, and LW_{reg}, with two versions of each chronology based on standardization with 30-year smoothing splines (GSF30) and 100-year smoothing splines described above (GSF100).

In addition to the newly developed longleaf pine chronologies, tree-ring width data from previously developed bald cypress trees (*Taxodium distichum*) growing at two nearby sites along the Withlacoochee River were collected from the International Tree-Ring Databank (Carr & Stahle, 2010; D. W. Stahle et al., 2010) (Figure 1). The bald cypress data included earlywood, latewood, and total ring width measurements, and we calculated a LW_{reg} series for each measurement series following the same methods as used for the longleaf pine (Griffin et al., 2011). Initial analyses indicated a common signal shared by the bald cypress trees from the two sites, which were therefore combined into a single set of measurement series for chronology development. In all, the bald cypress ring-width data included 74 measurement series from 34 trees and spanned 1516–2005, with an EPS>0.85 from 1650–2005 (Figure 3c). The bald cypress ring-width data exhibited few synchronous disturbance events and were therefore standardized to

develop eight total chronologies—four STD created using splines of 50% frequency cutoff at 100-year frequency to retain low-frequency growth patterns that could be linked to multi-decadal climate variability and four RES chronologies (TADI100; Figure 3c).

The complete set of chronologies included 16 longleaf pine chronologies and 8 bald cypress chronologies, each of which were clipped to the first year of a 50-yr window where the expressed population signal was >0.85 (Wigley et al., 1984) to ensure a robust signal for climate and growth analyses (Figure 3b, 3c). The standardization process was carried out using the computer program Arstan v44xp (Cook & Krusic, 2013).

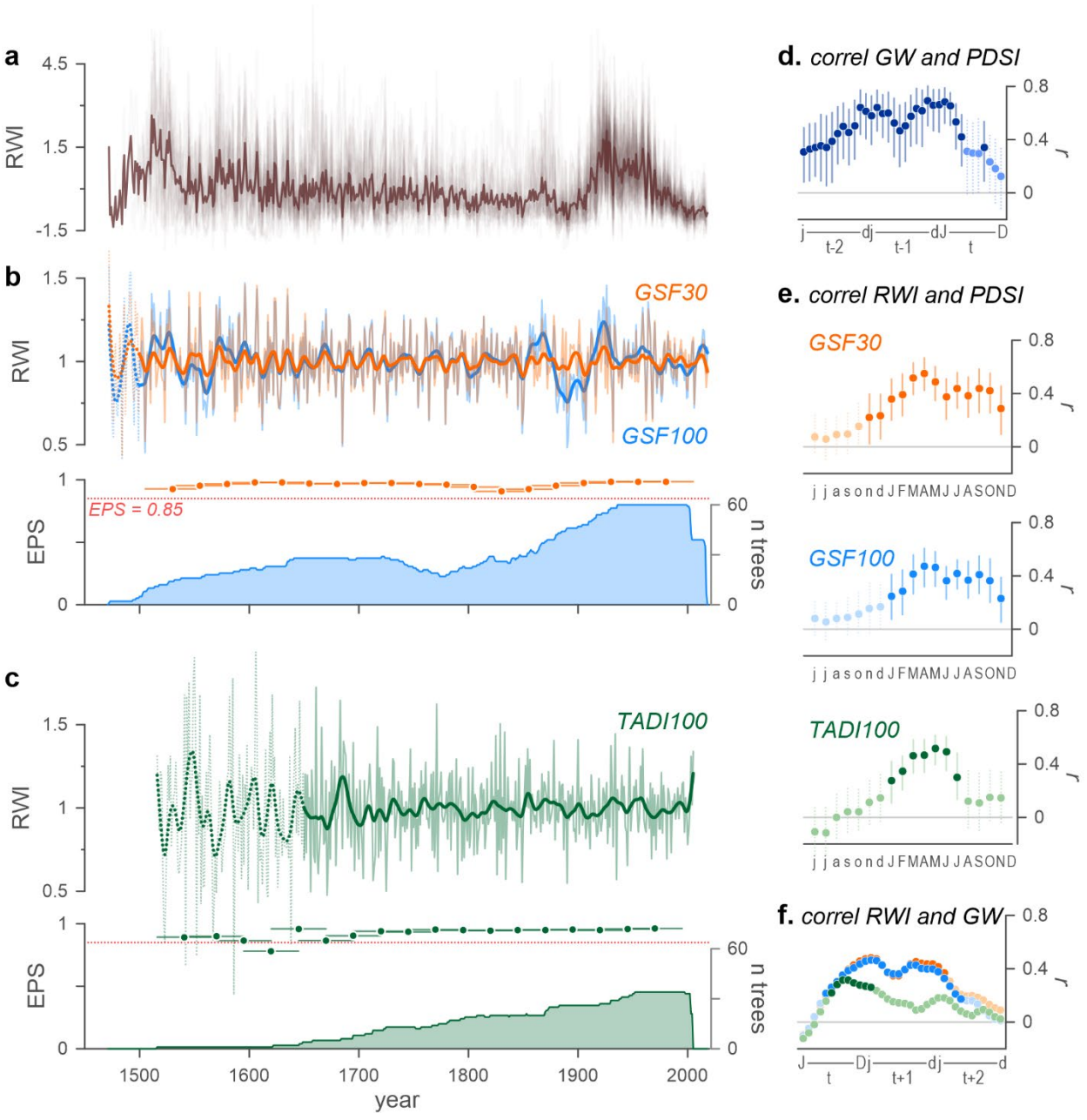

Figure 3. Linking tree growth to groundwater elevation. (a) Raw ring-width measurements of the 172 ring-width series from 91 longleaf pine trees and stumps sampled at Goethe State Forest, here normalized to a series mean of 0 with the sample-set mean shown in dark brown to illustrate a deep suppression that spanned the 1890s into the early 1900s that was followed by a sharp growth release that together likely represent land use changes associated with logging and turpentine operations at the site. (b) Two sets of standardized ring width-index chronologies for

the longleaf pine, here developed from total ring width, shown to illustrate the influence of land use on tree growth and how the applied standardization methods (GSF30 with its 30-year smoothing splines depicted in orange vs. GSF100 with its 100-year smoothing splines depicted in blue) retained more or less low-frequency information in the resulting chronologies; interannual chronology values are shown as thin lines with the chronologies smoothed using 15-year splines shown as bold; sample depth and expressed population signals indicate both chronologies are robust from 1505–2018 (EPS>0.85 where chronology lines are solid). (c) The standardized ring-width index chronology derived from bald cypress trees growing along the nearby Withlacoochee River (TADI100; green) shown as annual values (thin line) and smoothed with a 15-yr spline (bold line), EPS (EPS>0.85 where chronology lines are solid), and sample depth. (d) Correlation coefficients (symbol) and confidence intervals (whiskers) between mean annual groundwater elevation and monthly PDSI, from year t-2 to t, with bold colors indicating significant correlations (p<0.05). (e) Correlation coefficients and confidence intervals between each RWI chronology and monthly PDSI over the instrumental period, spanning from the previous year (lower case) to the current year (upper case), with bold colors indicating significant correlations (p<0.05). (f) Correlation coefficients between each of the total ring width RWI chronologies and mean monthly groundwater elevation over three years, from t to t+2, with bold colors indicating significant correlations (p<0.05).

2.4 Calibration, Verification, and Climate Reconstructions

Longleaf pine in this region of Florida are particularly sensitive to changes in hydrology because of the low water holding capacity of the sandy soils common to the region. Slight changes in depth to groundwater in such soils can have substantial effects on tree access to moisture

(Ciruzzi & Loheide, 2021; Foster & Brooks, 2001). Where access to groundwater does not directly impact tree growth, similar responses to precipitation and moisture balances may enable the identification of robust linkages between tree growth and groundwater elevation (Perez-Valdivia & Sauchyn, 2011). We therefore approached calibration of our tree-ring and groundwater data through a stepwise process that examined the environmental variables that could mechanistically link variability in tree growth and groundwater elevation. The relationships among these data were examined using correlation analyses as implemented in the dcc() function of the treeClim package of R (Zang & Biondi, 2015).

First, we compared the relationships among instrumental climate data and groundwater variability through correlation analysis of both monthly and seasonal variables. The data used in this analysis included monthly precipitation, maximum temperature, and Palmer's Drought Severity Index (PDSI) time series from 1895–2017 for NCDC Florida Division 3 (NCDC, 2018), and groundwater elevation above the National Geodetic Vertical Datum of 1929 measured on the 27th of each month near Newberry, Florida, at well S101722001 from 1959–2018 (Figure 1) (SRWMD, 2020). The USGS Newberry well was selected for its proximity to the study area and for the complete record it provided. The relationships among these data were examined for current and lagged relationships of up to two years using correlation analyses to identify links between atmospheric conditions and groundwater elevation. The strongest identified relationship between climate variables and groundwater elevation included a significant correlation between PDSI and groundwater elevation at up to a two-year lag, indicating persistence in the groundwater system (Figure 3d).

The climate responses of the 16 longleaf pine chronologies and 8 bald cypress chronologies exhibited similar overall relationships between tree growth and climate, with positive correlations to precipitation and PDSI and inverse relationships with maximum temperatures, though these varied by species and by the portion of the growth ring on which the chronologies were based (Figure S1). Differences in the seasonal timing of climate response were evident between EW and LW chronologies, and the window of climate response was narrower among the bald cypress chronologies than the longleaf pine chronologies (Figure S1). The strongest climate-growth relationships among all chronologies were consistently associated with PDSI (Figure 3e). This result supported the notion that soil moisture availability, as represented by PDSI, was directly related to both groundwater elevation and tree growth. Direct comparison of groundwater elevation and the tree-ring chronologies identified significant correlations that spanned windows of 8–25 months, with the strongest and most temporally expansive relationships identified with the longleaf pine chronologies (Figure 3f, Figure S2).

Based on the observed relationships among climate, tree growth, and groundwater, we created a final set of predictors for a regression-based reconstruction by identifying the common variance among those tree-ring chronologies that showed significant correlations to groundwater elevation. First, all chronologies were clipped to include only the period where subsample strength was >0.85, indicating a robust signal suitable for reconstruction (Buras, 2017). We then assembled two separate matrices of tree-ring chronologies, one based on the GSF30 and TADI100 chronologies and one based only on the GSF100 chronologies. Persistence in the groundwater system that created lagged climate-groundwater relationships (Figure 3d) and tree physiology that resulted in lagged climate-growth relationships (Figure 3e) were accounted for

by lagging the chronologies in each matrix from t-4 to t+4. The matrices were then refined by correlating each version of the chronologies with annual groundwater elevation at the USGS Newberry Well and retaining only those that exhibited significant Pearson product moment correlations ($p < 0.01$). The first matrix spanned 1695–2002 and included 10 chronologies, five from the GSF30 and four from the TADI100 data sets. The second matrix spanned 1498–2015 and included nine chronologies from the GSF100 data. We reduced the multicollinearity in each matrix using principle components analysis (PCA) as implemented by the prcomp() function in R (R Development Core Team, 2019).

The principle components (PCs) derived for each matrix were considered in the development of two linear regression models using a forward and backward selection stepwise procedure as implemented in the step() function of R (R Development Core Team, 2019). The resulting reconstructions were assessed through a split calibration and verification process on the early and late halves of each calibration period using the skill() function in the R package treeClim (Zang & Biondi, 2015), rescaled to the instrumental record, and examined for potential bias using an extreme value capture test (McCarroll et al., 2015).

The final GSF100 regression model explained 60% of the variance in mean annual instrumental groundwater elevation at the Newberry Well from 1959–2015, and the GSF30+TADI100 reconstruction explained 60% of the variance in instrumental annual groundwater elevation from 1959–2002 (Figure 4a). Both reconstructions were skillful, with reduction of error statistics of 0.62–0.69 (Table 1). The coefficient of efficiency (CE) was positive in all cases, though it was close to zero when calibrated on the early split of the GSF100 reconstruction (Table 1). Of note,

379 when calibration and verification of the GSF100 reconstruction were conducted over the same
380 period as the GSF30+TADI100 reconstruction (1959–2002), CE was strongly positive for both
381 splits (see $GSF100_{trim}$ in Table 1). Durbin-Watson *d* statistics were significant for all but the
382 GSF100 late split based on the shortened calibration window which indicated significant
383 autocorrelation in the model residuals. Visual inspection of the model showed the tree-ring
384 reconstructions over-estimated groundwater elevation in more recent decades (Figure 4a).
385 Comparing first-difference time series of both the instrumental and reconstructed time series
386 indicated significant predictive power in the reconstructions even when trend was removed
387 (Figure 4a). These results collectively indicate that useful information is provided by these
388 reconstructions and also suggest the influence of a driving factor that affected groundwater
389 elevation but not tree growth over the most recent decades.
390
391 The two reconstructions were complementary. The reconstruction based on the
392 GSF30+TADI100 chronologies did not extend as far into the past or as close to the present but
393 retained low frequency variability most likely related to climate from the TADI100 chronologies,
394 while the GSF30 chronologies contributed information about high-frequency variability with
395 minimal influence of the late 1800s turpentine industry/land use signal (Figure 4b). The
396 reconstruction based on the GSF100 chronologies extended further into the past and closer to the
397 present, but due to the more conservative standardization retained low frequency variability in
398 the late 1800s and early 1900s that represented land use influences and not climatic information
399 (Figure 4b). Analysis of the extreme value capture (McCarroll et al., 2015) indicated that both
400 the GSF30+TADI100 and the GSF100 reconstructions exhibited biases toward better
401 representation of extreme high groundwater elevation (EVC = 3/4 and 4/6, respectively, both $p <$

0.01) as compared to extreme low elevation (EVC = 2/4 and 2/6). This wet-bias is unusual among tree-ring-based hydrologic reconstructions that often better represent dry conditions (Wise & Dannenberg, 2019). This result could be explained by the persistence in groundwater elevations, where the relatively open groundwater aquifer created by the extremely well-drained sandy soils of the site may smooth out the effects of short-duration, extreme rainfall events that are often missed by trees growing in arid conditions. Alternatively, the asymmetry could be explained by non-climatic factors. All of the groundwater elevations within the 10^{th} lowest percentile in the instrumental record occurred since 2001, the period of greatest potential impacts from groundwater extraction. Extreme lows in groundwater elevation driven in part by human factors would be absent in tree-ring records that more purely express climate drivers. Regardless of the reasons behind the asymmetrical extreme capture characteristics of the chronologies, the overall similarity in response of the two chronologies supported creation of a spliced reconstruction by adding the early and late portions of the GSF100 reconstruction onto the GSF30+TADI100 reconstruction. The resulting spliced chronology explained 63% of the variance in mean annual instrumental groundwater elevation and retained low-frequency signal throughout while minimizing the potential influence of land use in the 1800s (Figure 4a, 4c).

As a final assessment of the spliced reconstruction, we compared the spatial footprints of instrumental and reconstructed groundwater elevation responses to drought and sea surface temperatures using KNMI Climate Explorer (Trouet & Van Oldenborgh, 2013). Spatial correlations with drought showed responses centered on northern Florida (Figure 5a), while correlations with sea surface temperatures depicted a clear relationship with El Niño-Southern Oscillation variability over the instrumental period (Figure 5b). Although both spatial signatures

were somewhat weaker with the reconstruction than the instrumental data, the geographic extent and strength of the correlations were generally similar, broadly supporting the skill of the reconstruction (Tegel et al., 2020).

Table 1. Calibration and verification statistics for reconstructing mean annual groundwater elevation in North Central Florida. The $GSF100_{trim}$ model results are based on the same calibration window as the GSF30+TADI100 model. The spliced reconstruction includes the GSF30+TADI100 model for years 1959–2002 and the GSF100 model for years 2003–2015.

Reconstruction	Calibration period	Validation period	r^2	RE	CE	*d*
GSF100	1959–2015		0.60			
	1959–1987	1988–2015	0.55	0.62	0.03	1.21*
	1988–2015	1959–1987	0.55	0.69	0.26	1.30*
$GSF100_{trim}$	1959–2002		0.57			
	1959–1980	1981–2002	0.57	0.61	0.26	1.04*
	1981–2002	1959–1980	0.61	0.53	0.52	1.71
GSF30+TADI100	1959–2002		0.60			
	1959–1980	1981–2002	0.64	0.62	0.45	0.99*
	1981–2002	1959–1980	0.50	0.69	0.56	0.90*
Spliced reconstruction	1959–2015		0.63			

* indicates $p < 0.05$

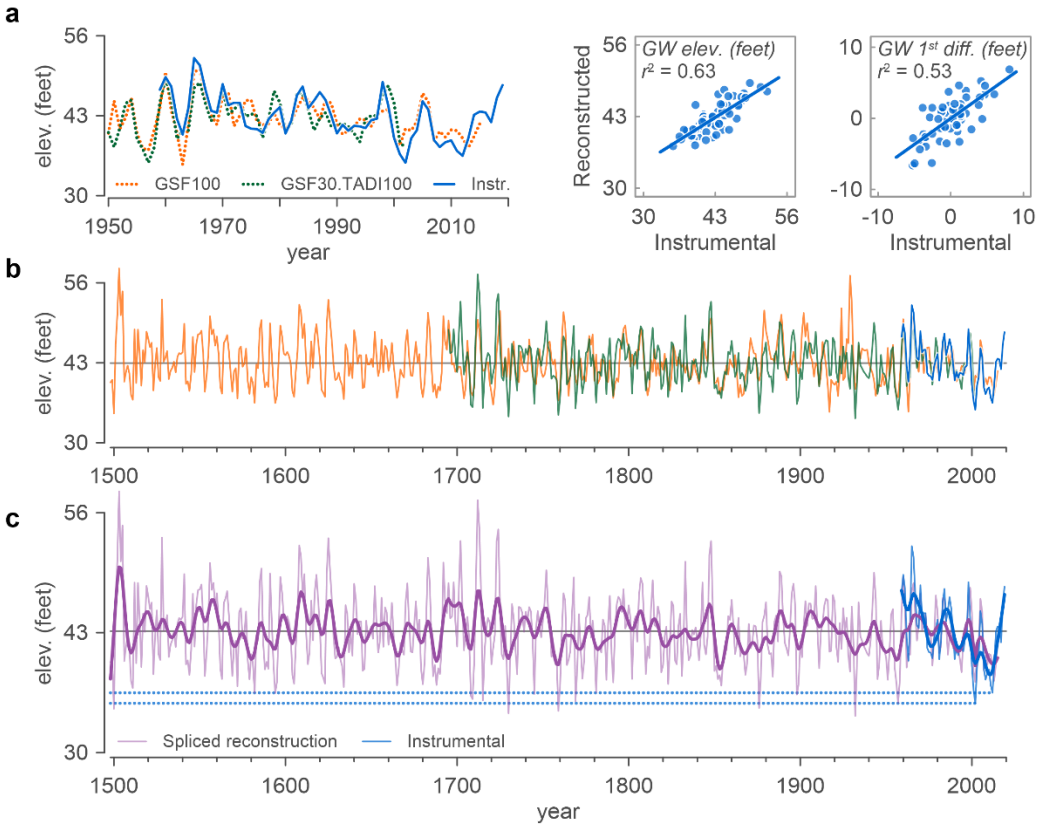

Figure 4. Calibration, verification, and reconstruction of mean annual groundwater elevation for the Newberry USGS Well in North Central Florida. (a) Comparison of two versions of the reconstruction (GSF100 only, GSF30+TADI100) with instrumental mean annual groundwater elevation, along with scatter plots comparing the spliced reconstruction and instrumental groundwater elevation. A similar scatter plot based on first-differenced versions of the reconstruction and instrumental record is presented to specifically compare the high-frequency patterns of the time series. (b) The full GSF100 and GSF30+TADI100 reconstructions along with the instrumental record. (c) The final spliced reconstruction shown relative to the instrumental record, both with 15-yr smoothing splines to emphasize lower-frequency variations in groundwater elevation. Thin horizontal dotted lines are included to compare extreme individual-year lows in the instrumental record to the longer-term reconstruction.

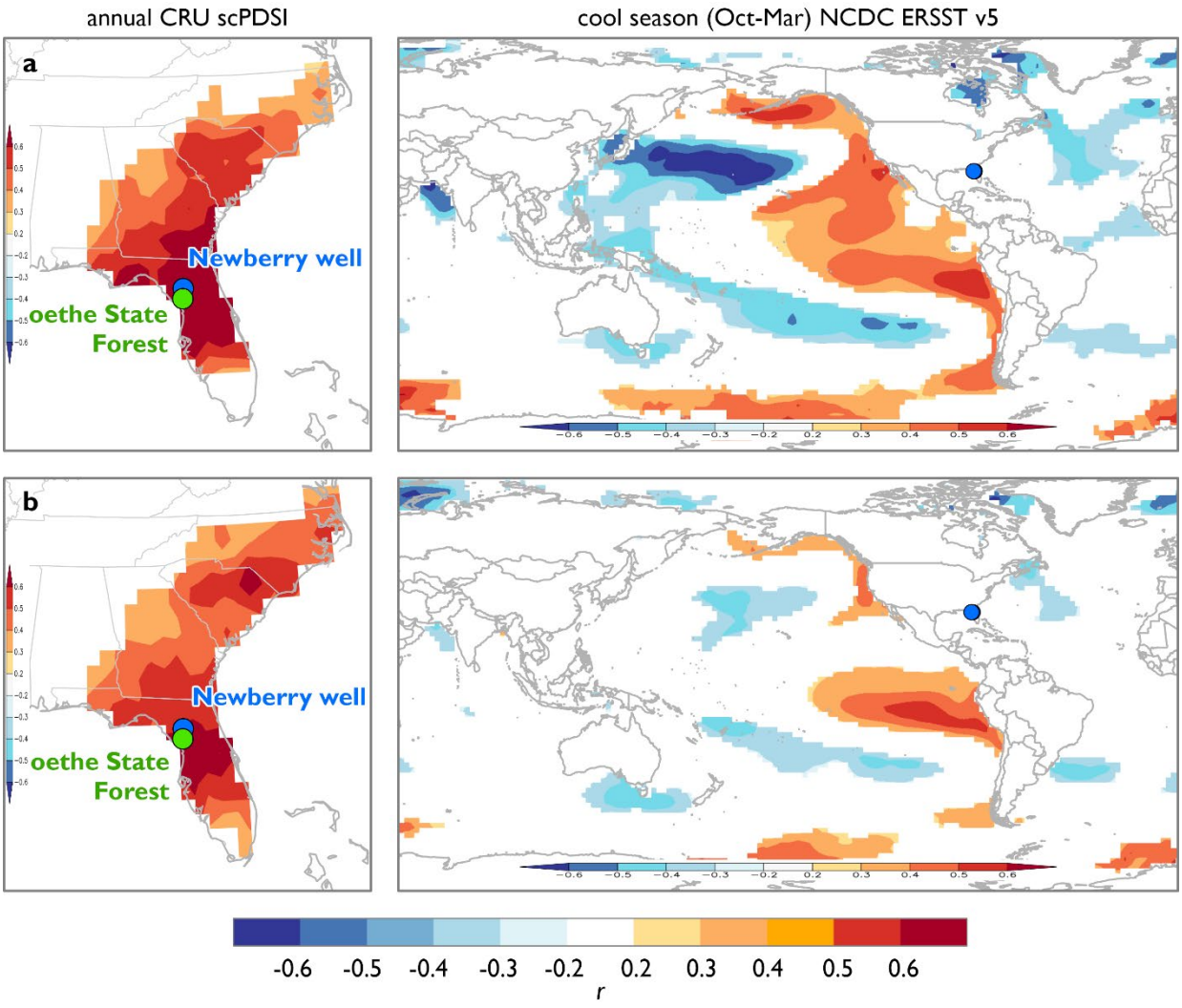

448

449 **Figure 5.** Spatial climate response of instrumental and reconstructed groundwater elevation.
450 Correlation of (a) instrumental and (b) reconstructed annual groundwater elevation with drought
451 (scPDSI, 1959–2015) and sea surface temperatures (ERSST v5, 1977–2015). Correlations with
452 sea surface temperatures were stratified based on shifting relationships with ocean conditions
453 over time, as detailed below.

454

455 ## 2.5 Interpreting the reconstruction: long-term variability in groundwater resources

456 The spliced reconstruction of mean annual groundwater elevation at the USGS Newberry well
457 presented here extends information on groundwater elevation over 450 years beyond the
458 instrumental record of the well, and over 400 years beyond any instrumental groundwater record
459 in Florida. This expanded temporal perspective allows modern events to be viewed in the context
460 of long-term variability; however, the calibration and verification results require additional
461 consideration regarding the differing CE results for the GSF100 reconstruction when the most
462 recent two decades are included in the calibration and the significant residuals in each version of
463 the reconstruction. Comparing groundwater elevations recorded at the USGS Newberry well to
464 those recorded at the Cross City well supports the notion that these results represent a dampening
465 of the linkages that connect atmospheric conditions, tree rings, and groundwater elevations as the
466 influences of groundwater extraction increase.
467
468 The Cross City well is located at the landward edge of Florida's Big Bend coastal zone, which,
469 until somewhat recently, has been one of the least developed coastal regions of the United States
470 (Volk et al., 2017). The Cross City well is thus more distant from urban centers and areas of
471 intense agricultural groundwater use, making it less likely to be influenced by groundwater
472 extraction (Figure 1), and while the numerous missing observations early in the record limit its
473 usefulness as a target for calibration and reconstruction, the data do offer insight for interpreting
474 the Newberry reconstruction. Comparing z scores for instrumental mean annual groundwater
475 elevations at the Cross City and Newberry wells identifies an increasing difference between
476 groundwater elevations at the two sites over time that is more pronounced during years of low
477 groundwater (Figure 6a, 6b). This pattern matches both observed and modeled impacts of

groundwater withdrawals on regional groundwater elevations (Gordu & Nachabe, 2021). Comparing the difference between the two well records to the Newberry reconstruction residuals, with both transformed into z scores, shows a similar increasing trend over time (Figure 6c). Taken together, and in the context of known increases in groundwater extraction (Marella & Berndt, 2005), the increasing difference between groundwater elevation at the Cross City and USGS Newberry wells and the overestimation of recent groundwater elevation in the Newberry reconstruction represent a weakening of climatic control over groundwater elevation that is likely unprecedented. This also suggests that future low groundwater elevation will be amplified by groundwater extraction, increasing the probability of water resource scarcity beyond what has been experienced in at least the past 500 years.

The implications for interpreting the overall reconstruction are substantial, but do not undermine the value of the results reported here. Given the relatively recent development of high-capacity wells in the vicinity of the USGS Newberry well, and supported by data from modeling efforts, it is likely that substantial human impacts on groundwater elevation began in the 1990s and have increased since that time (Gordu & Nachabe, 2021). This means the calibration dataset provides at least three decades of relatively stable relationships among climate, groundwater elevation, and tree growth. The weakening of these relationships and amplified declines in groundwater elevation over recent decades, when included in the calibration and particularly when used to rescale the reconstruction, could bias the overall mean of the reconstruction. However, the strong relationship between the first-differenced instrumental and reconstructed time series and the similar spatial climate responses suggest that the reconstruction accurately captures interannual variability in groundwater elevation. Based on the assumption of stable climate-groundwater-tree

growth relationships prior to the period of groundwater extraction, we suggest that the reconstruction presented here is a valid representation of pre-instrumental groundwater elevation.

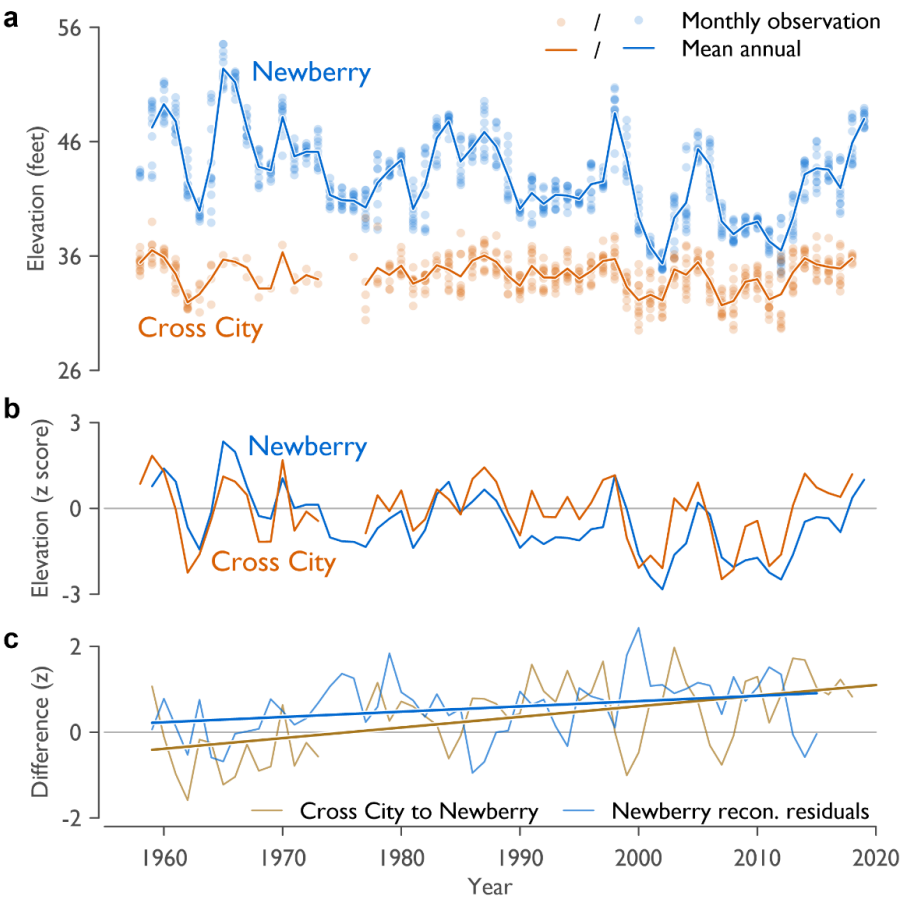

Figure 6. Groundwater elevations at two wells in North Central Florida illustrate regionally declining groundwater levels. (a) Observed mean annual groundwater elevations at the USGS Newberry and Cross City wells. (b) Z scores of mean annual groundwater elevations for both wells illustrating how the USGS Newberry instrumental measurements trend lower than those of the Cross City well since ca. 1990. (c) Trend in the difference between instrumental groundwater elevations at the Cross City well and the USGS Newberry well are similar to the Newberry reconstruction residuals, reflecting the possible impacts of extraction on groundwater elevations at the USGS Newberry well.

513 Given the considerations outlined above, the reconstruction of mean annual groundwater
514 elevation at the USGS Newberry well provides important historical context for modern
515 hydrologic conditions. First, as is the case with nearly all proxy-based hydrologic
516 reconstructions, the distribution of reconstructed annual groundwater elevation for the
517 instrumental period does not match the range of conditions represented over the full length of the
518 reconstruction (Figure 7a). Reconstructed single year extreme lows and highs surpass the most
519 extreme conditions observed since the start of direct groundwater elevation monitoring (Table 2)
520 and suggest caution in basing long-term forecasts of water availability on the historical record
521 (Pederson et al., 2012). Individual years and extended pluvial conditions in the mid-1500s, early
522 1600s, and early 1700s exhibited higher groundwater elevations than experienced at any point in
523 the instrumental period. At the same time, the low instrumental groundwater elevations recorded
524 in 2002 and 2012 are among the lowest 5% of reconstructed groundwater elevations in the past
525 500 years (Figure 4c, Table 2). The same years in the reconstruction are within the lowest 6%,
526 and 15%, respectively—low, but not as extreme.
527
528 The more extreme ranking of these years based on instrumental records may be related to the
529 extreme capture characteristics of the reconstruction, in that proxy-based records do not readily
530 represent the most extreme conditions of the target variable (McCarroll et al., 2015). If that is the
531 case, it would suggest that past lows in groundwater elevation in the reconstruction
532 underestimate actual elevation and therefore serve as a conservative estimation of worst-case
533 conditions. An alternative interpretation is that the reconstruction accurately represents the
534 climatological influences on groundwater elevation and that groundwater extraction amplified
535 these lows to extreme levels over recent decades. If true, this suggests that not only are the return

of extreme low groundwater conditions unavoidable due to climate variability, but that these conditions will be amplified by current and ongoing groundwater extraction. This increases the likelihood of North Central Florida experiencing more severe water deficits than experienced in the instrumental period thus far.

Building on the perspective gained from individual years, considering the consecutive number of years of above or below average groundwater elevation, or runs, provides a useful perspective on the duration of high- or low-groundwater conditions. We calculated runs relative to the mean of the full reconstruction ($\bar{x}$ = 43.14 feet above the National Geodetic Vertical Datum of 1929 from 1498–2015) as a way to further place recent groundwater elevations in a long-term context (Figure 7b). The median run length was 2 years for both above- and below-average groundwater elevations, suggesting ground water elevations were primarily characterized by high-frequency variability; however, this was not consistent through time. Periods of more persistent above- and below-average conditions occurred at several points in the reconstruction, including from the mid-1500s through the early 1600s, and at approximately 50–70-year intervals from ca. 1700 through 2000 (Figure 7b). The longest distinct run for above-average conditions relative to the long-term record was 10 years long and spanned 1791–1801, while the longest below-average runs included two 9-year periods of low groundwater from 1989–1997 and from 2007–2015.

Shifting levels of persistence in the reconstruction suggests shifting climate drivers of groundwater elevation. To supplement the runs analysis, we examined the power spectra of the reconstruction using a continuous Morlet wavelet transform calculated by the morlet() function in dplR (Bunn, 2008; Torrence & Compo, 1998). Significant periodicities at 5–15 years

559 identified throughout the 1500s into the early 1600s, again in the late 1600s into the mid-1700s,
560 and sporadically throughout the 1800s and 1900s (Figure 7c) generally align with the periods of
561 greater persistence identified in the runs analysis (Figure 7b). Significant periodicity in the ca.
562 100-year band is evident from the 1600s through the 1900s and again aligns with peaks in
563 persistence in the runs analysis centered on the years 1600, 1700, 1800, 1900, and possibly 2000.
564 Interpretation of this response is problematic as frequencies above 100 years were largely
565 removed from the tree-ring chronologies via standardization (Figure 7c). Collectively,
566 interpretation of the runs and wavelet spectra suggest an important role in groundwater
567 elevations for climate drivers that exhibit oscillatory behaviors, but that the influences of these
568 factors wax and wane through time.
569
570 The expression of shifting persistence in groundwater elevation variability is illustrated by
571 considering cumulative anomalies, defined here as the sum of annual groundwater elevation
572 anomalies over continuous periods of above- or below-average groundwater elevation relative to
573 the reconstruction mean. Periods of low persistence such as those in the mid-1600s and early
574 1800s generally aligned with near-average groundwater elevations, while periods of greater
575 persistence coincided with deep pluvial or drought conditions (Figure 7d). For example,
576 cumulative anomalies of below-average groundwater elevations clustered in the late 16th century,
577 which is a period of megadrought documented across much of North America (David W. Stahle
578 et al., 2007). In this context, recent cumulative anomalies of below-average groundwater
579 elevations, driven in part by the rise in persistence over recent decades, were surpassed only once
580 in the past 500 years (Figure 7c, 7d). Furthermore, the overestimation of groundwater elevation
581 for recent decades of the reconstruction (Figure 6) suggests that while hydrologic drought

582 contributed to recent declines in groundwater elevation across the southeastern United States
583 (Vines et al., 2021), the potential amplification of these declines by groundwater extraction likely
584 resulted in the some of the lowest groundwater elevations in at least the past 500 years (Figure
585 4c, 7d).

586

587 **Table 2.** Years of extreme reconstructed groundwater elevations

Years of extreme low groundwater				Years of extreme high groundwater			
Reconstructed		Observed		Reconstructed		Observed	
year	Elevation (ft)	year	Elevation (ft)	year	Elevation (ft)	year	Elevation (ft)
1932	34.0	2002	35.4	1503	58.3	1965	52.4
1730	34.3	2012	36.5	1712	57.4	1966	51.2
1759	34.5	2001	36.8	1724	54.2	1960	49.3
1500	34.8	2011	37.3	1713	54.1	1998	48.5
1876	34.8	2008	37.9	1505	54.6	1970	48.1
1957	35.4	2009	38.7	1702	52.9	2019	48.0
1769	35.6	2010	39.0	1848	52.9	1961	47.8
1715	35.6	2007	39.0	1723	52.9	1984	47.7
1709	35.8	2003	39.3	1528	53.3	1959	47.2
1708	36.2	2013	39.3	1625	53.2	1967	47.2
1898	36.3	2000	39.4	1608	52.5	1987	46.8
1745	36.4	1963	40.0	1847	51.4	1983	46.3
1594	36.5	1981	40.1	1609	51.3	2018	45.9
1582	36.5	1990	40.1	1683	51.1	1988	45.6
1781	36.5	1977	40.2	1833	50.7	1986	45.5

588

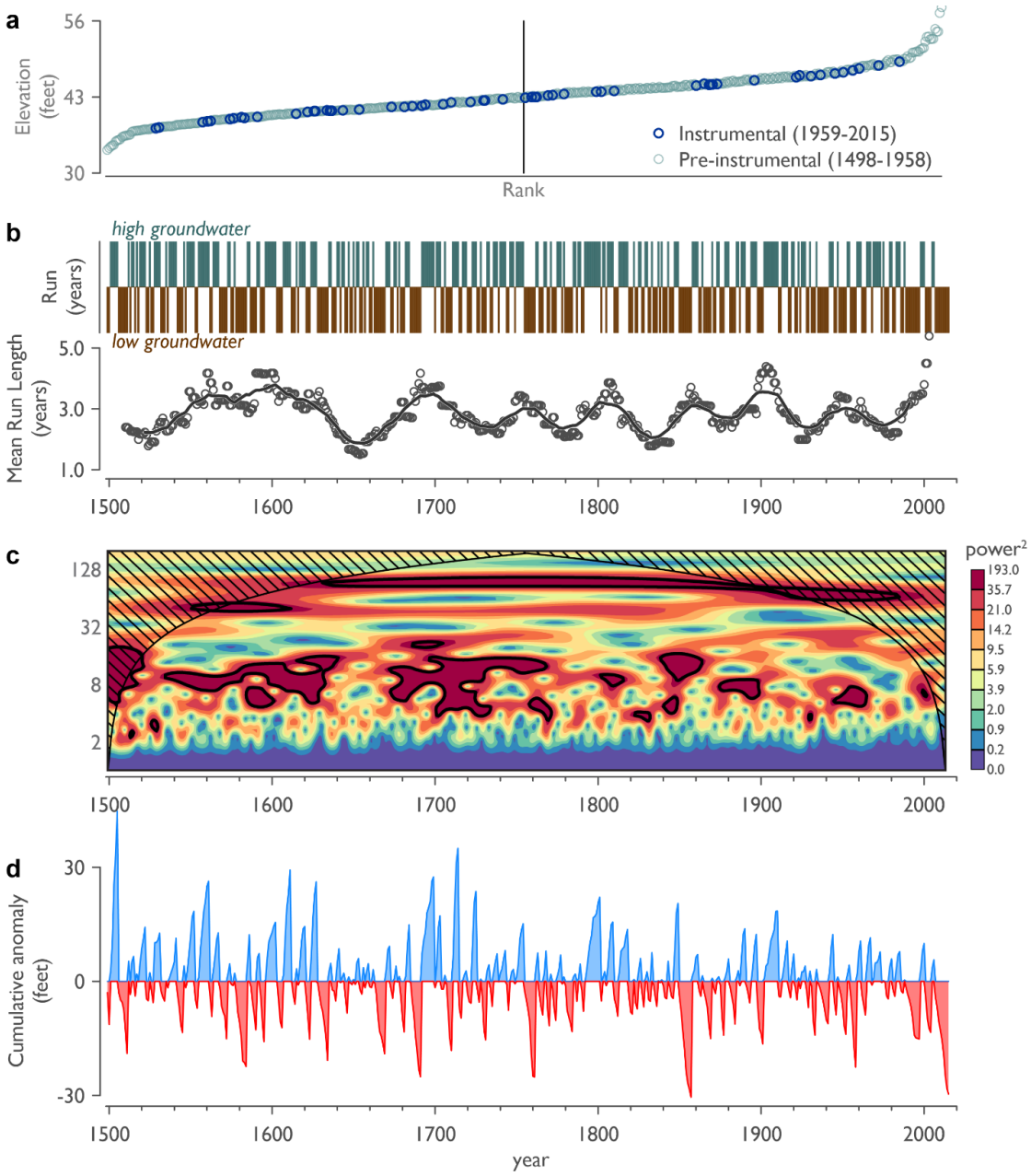

Figure 7. Analysis of reconstructed groundwater elevation. (a) A ranked distribution of groundwater elevation depicting the reconstructed values during the instrumental period relative to the entire reconstruction. (b) Runs of consecutive years above- or below-average groundwater elevations relative to the mean of the full reconstruction (1498–2015) shown as unique events (top) and as a moving 25-yr average of the length of each run, regardless of the associated sign, fit with a 25-year moving average for illustration purposes. (c) Wavelet power spectra of the

596 spliced groundwater reconstruction for North Central Florida. Black contours indicate significant
597 power (p<0.05). Cross-hatched regions are the cone of influence where spectra may be distorted
598 due to edge effects. (d) Cumulative anomalies shown as the sum of consecutive anomalies in
599 each run of above- or below-average groundwater elevations.
600
601

602 2.6 Considering the influences of oceanic-atmospheric phenomena on groundwater

603 In Florida, multiple oceanic-atmospheric phenomena interact to influence patterns of
604 atmospheric circulation that, in turn, drive hydrological variability and groundwater conditions.
605 These include the El Niño-Southern Oscillation (ENSO) and the Atlantic Multidecadal
606 Oscillation (AMO), both of which may be modulated through interactions with sea surface
607 temperatures in the north Pacific (Enfield et al., 2001; McCabe et al., 2008; McCabe et al., 2004;
608 Tootle & Piechota, 2006). Although the impacts of these phenomena are documented over the
609 instrumental record, their influence on the climate of northern Florida is variable over time,
610 particularly with respect to ENSO (Cole & Cook, 1998; Torbenson et al., 2019). The significant
611 band of 5–15 year periodicity identified through much of the reconstruction encapsulates ENSO-
612 scale forcing (Cane, 1986), as well as longer-term variability, while the 100-yr periodicity
613 identified in the reconstruction surpasses the canonical description of AMO variability (Enfield
614 et al., 2001; Newman et al., 2016). It is noteworthy that neither of these modes of variability in
615 the reconstruction precisely fit the observed scale at which these coupled oceanic-atmospheric
616 phenomena operate, and yet consistent patterns of increasing and decreasing persistence exist in
617 the reconstruction that reflect the oscillatory behavior associated with these processes. This
618 suggests the existence of inter-basin interactions of oceanic-atmospheric processes that drive the

619 periodicity and variable persistence in groundwater elevations at our site. This is illustrated by
620 examining the relationship between the reconstruction and global sea surface temperatures over
621 time.
622
623 Correlations between the groundwater reconstruction and global SST (NCDC ERSST v5, Huang
624 et al., 2017), calculated and visualized using KNMI Climate Explorer (Trouet & Van
625 Oldenborgh, 2013), illustrate modulation of ENSO influences over time by contingent phases of
626 the AMO and PDO (Dong et al., 2006; Li et al., 2013; Yeh & Kirtman, 2005). The influence of
627 ENSO on groundwater elevation was strongest during periods of contrasting AMO and PDO
628 phases and diminished during periods of coherent phases of these coupled oceanic-atmospheric
629 phenomena (Figure 8). The temporal scope of this analysis was extended beyond the period of
630 instrumental sea surface temperature records by comparing the groundwater elevation
631 reconstruction to a suite of proxy-based reconstructions of ENSO variability that were variously
632 based on tree-ring and coral records (Datwyler et al., 2019; Freund et al., 2019; Li et al., 2013;
633 D. W. Stahle et al., 1998; Torbenson et al., 2019). Moving correlations over 25-year windows
634 indicated widely varying relationships between groundwater elevation and each representation of
635 ENSO activity (Figure 9). Taken together, these results underscore that northern Florida is within
636 a region of intersection among multiple climate driver impacts (Maleski & Martinez, 2018), and
637 that while this produces inconsistent patterns of teleconnection influences through time, the
638 longer-term perspective of groundwater elevations enabled through this tree-ring-based
639 reconstruction helps identify patterns in groundwater conditions that may prove helpful for
640 groundwater resource projects. Specifically, understanding how the sea surface temperatures
641 associated with contrasting phases of the AMO and PDO influence atmospheric circulation to

amplify ENSO influences on groundwater resources in northern Florida could enable forecasting persistence and the likelihood of long-term water abundance or scarcity.

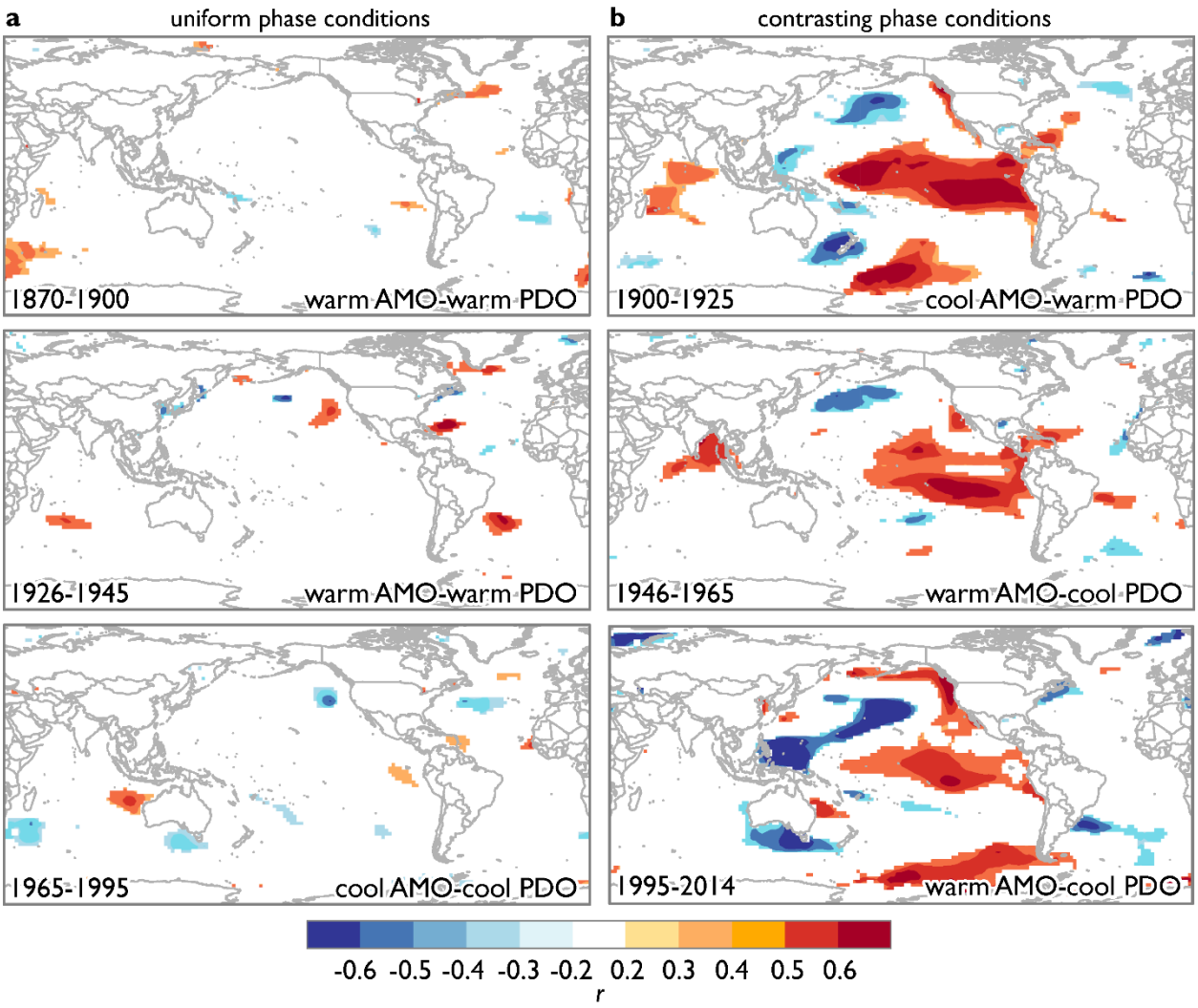

Figure 8. Shifting relationships between sea surface temperatures (SST) and reconstructed groundwater elevation in North Central Florida. Correlations between annual groundwater elevation and December–March NCDC ERSST v5 sea surface temperatures during (a) periods of similar AMO and PDO phases and (b) periods of contrasting AMO and PDO phases illustrate a temporally variable influence of ENSO on North Central Florida hydrologic conditions.

652

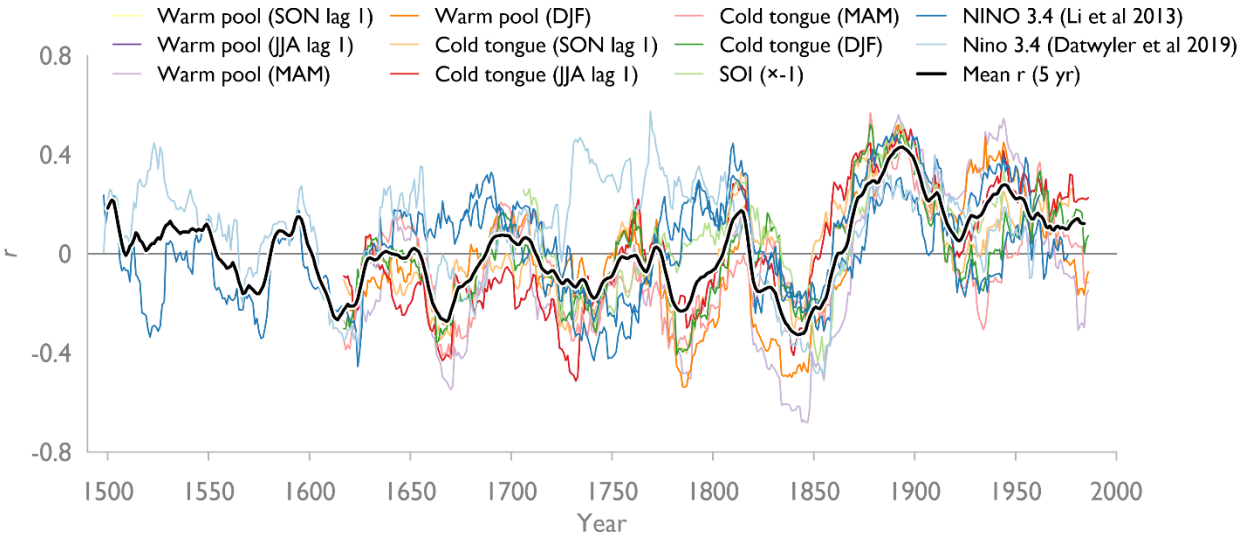

653

654 **Figure 9.** Relationship between reconstructed North Central Florida groundwater and a suite of
655 proxy-based reconstructions of different aspects of El Niño-Southern Oscillation variability.
656 Values are the Pearson product moment correlation coefficient for the first year of moving 30-
657 year windows.

658

659

660 **3. Conclusions**

661 The reconstruction we report here expands tenfold the temporal perspective on groundwater
662 variability in North Central Florida. In doing so, we identified a high likelihood of recent low
663 groundwater elevations that reached levels comparable to past megadrought periods and suggest
664 that groundwater extraction likely magnified the influence of climate to drive these extreme
665 lows. Collectively, our results illustrate the cross-scale interactions of inter-basin oceanic-
666 atmospheric teleconnections that modulate the influence of ENSO variability on northern Florida
667 hydroclimate variability. These climate drivers create periods of greater and less persistence

668 within groundwater elevations that in turn produce prolonged periods of near-average conditions
669 when persistence is low and pluvial or deep drought when persistence is high. Based on the past
670 500 years of groundwater elevations, it appears that persistence is currently increasing and will
671 likely do so for at least another decade. This suggests that water resource managers would do
672 well to plan for sustained conditions that could continue current droughts or cause a switch to a
673 prolonged pluvial. The amplification of future drought conditions by groundwater extraction will
674 lead to water scarcity at levels not observed during the instrumental period.

675

676 **Acknowledgments**

677 Thanks go to Nick Flinner for his steadfast work developing initial tree-ring chronologies from
678 old longleaf pine stumps, Zach Holmboe and Sam Horsnell for their assistance in the field, Fay
679 Baird for help in the field and gathering and collating groundwater well data, and Mark Larson
680 for his assistance in identifying sampling areas and understanding the history of Goethe State
681 Forest. Neil Pederson provided insightful comments on an earlier version of this manuscript that
682 helped refine our approach to reconstructing groundwater variability. Funding for this research
683 was provided by the Suwannee River Water Management District. The authors declare no real or
684 perceived conflicts of interest.

685

686 **Open Research**

687 Upon acceptance for publication, all tree-ring data developed for this study will be made publicly
688 accessible through the International Tree-Ring Data Bank [available:
689 https://www.ncei.noaa.gov/products/paleoclimatology/tree-ring], with the following statement
690 then relevant:

691

692 The tree-ring data used in the groundwater reconstruction are available at the International Tree-
693 Ring Data Bank (https://www.ncei.noaa.gov/products/paleoclimatology/tree-ring) via [link;
694 Goethe State Forest longleaf pine chronologies], [link2; Bald cypress chronologies], and [link3;
695 Bald cypress chronologies]. Instrumental groundwater data used are available through the My
696 Suwannee River Water Management District portal
697 (https://www.mysuwanneeriver.com/108/Groundwater-Levels) via
698 [http://www.mysuwanneeriver.org/data/GWData/S101722001/S101722001_Level.xlsx;
699 Newberry] and
700 [http://www.mysuwanneeriver.org/data/GWData/S101210001/S101210001_Level.xlsx; Cross
701 City]. Figures were created using Grapher v15 software (https://www.goldensoftware.com) and
702 maps were created in ArcGIS Pro v2.4 (https://www.esri.com).

703

704

705 **References**

706 Barlow, P. M. (2003). *Ground Water in Freshwater-Saltwater Environments of the Atlantic Coast*.
707 Reston, Virginia: U.S. Geological Survey Circular 1262.
708 BEBR. (2011). *Florida estimates of population 2010*. Retrieved from University of Florida Bureau
709 of Economic and Business Research, Gainesville, Florida:
710 https://www.bebr.ufl.edu/population_repo_cats/florida-population-estimates/
711 BEBR. (2020). *Florida estimates of population 2020*. Retrieved from University of Florida Bureau
712 of Economic and Business Research, Gainesville, Florida:
713 https://www.bebr.ufl.edu/population_repo_cats/florida-population-estimates/

714 Bierkens, M. F. P., & Wada, Y. (2019). Non-renewable groundwater use and groundwater
715 depletion: a review. *Environmental Research Letters, 14*(6), 063002.
716 https://doi.org/10.1088/1748-9326/ab1a5f
717 Bunn, A. G. (2008). A dendrochronology program library in R (dplR). *Dendrochronologia, 26*,
718 115–124. https://doi.org/10.1016/j.dendro.2008.01.002
719 Buras, A. (2017). A comment on the expressed population signal. *Dendrochronologia, 44*, 130–
720 132. https://doi.org/10.1016/j.dendro.2017.03.005
721 Cane, M. A. (1986). El Niño. *Annual Review of Earth and Planetary Sciences, 14*, 43–70.
722 https://doi.org/10.1146/annurev.ea.14.050186.000355
723 Carr, D., & Stahle, D. W. (2010). *NOAA/WDS Paleoclimatology - Carr - MIddle Withlacoochee*
724 *River - TADI - ITRDB FL008*. NOAA National Centers for Environmental Information.
725 https://doi.org/10.25921/gqph-x765. Accessed June 15, 2019.
726 Ciruzzi, D. M., & Loheide, S. P. (2021). Groundwater subsidizes tree growth and transpiration in
727 sandy humid forests. *Ecohydrology, 14*(5). https://doi.org/10.1002/eco.2294
728 Cole, J. E., & Cook, E. R. (1998). The changing relationship between ENSO variability and
729 moisture balance in the continental United States. *Geophysical Research Letters, 25*(24),
730 4529–4532. https://doi.org/10.1029/1998GL900145
731 Cook, E. R. (1985). *A Time Series Analysis Approach to Tree Ring Standardization.* (Ph.D. Ph.D.
732 Dissertation), University of Arizona, Tucson, Arizona.
733 Cook, E. R., & Krusic, P. J. (2013). ARSTAN v44h2: A tree-ring standardization program based
734 on detrending and autoregressive time series modeling, with interactive graphics.
735 Palisades, New York, USA: Tree-Ring Laboratory, Lamont-Doherty Earth Observatory of
736 Columbia University.

737 Cook, E. R., & Peters, K. (1981). The smoothing spline: a new approach to standardizing forest
738 interior tree-ring width series for dendroclimatic studies. *Tree-Ring Bulletin, 41*, 45–53.
739 http://hdl.handle.net/10150/261038
740 Cook, E. R., & Peters, K. (1997). Calculating unbiased tree-ring indices for the study of climatic
741 and environmental change. *The Holocene, 7*(3), 361–370.
742 https://doi.org/10.1177/095968369700700314
743 Crockett, K., Martin, J. B., Grissino-Mayer, H. D., Larson, E. R., & Mirti, T. (2010). Assessment
744 of tree rings as a hydrologic record in a humid subtropical environment. *Journal of the*
745 *American Water Resources Association, 46*(5), 919–931. https://doi.org/10.1111/j.1752-
746 1688.2010.00464.x
747 Datwyler, C., Abram, N. J., Grosjean, M., Wahl, E. R., & Neukom, R. (2019). El Nino-Southern
748 Oscillation variability, teleconnection changes and responses to large volcanic eruptions
749 since AD 1000. *International Journal of Climatology, 39*(5), 2711–2724. Article.
750 https://doi.org/10.1002/joc.5983
751 de Graaf, I. E. M., Gleeson, T., van Beek, L. P. H., Sutanudjaja, E. H., & Bierkens, M. F. P. (2019).
752 Environmental flow limits to global groundwater pumping. *Nature, 574*(7776), 90–94.
753 http://dx.doi.org/10.1038/s41586-019-1594-4
754 Dong, B. W., Sutton, R. T., & Scaife, A. A. (2006). Multidecadal modulation of El Niño-Southern
755 Oscillation (ENSO) variance by Atlantic Ocean sea surface temperatures. *Geophysical*
756 *Research Letters, 33*(8), L08705. Article. https://doi.org/10.1029/2006gl025766
757 Enfield, D. B., Mestas-Nunez, A. M., & Trimble, P. J. (2001). The Atlantic multidecadal
758 oscillation and its relation to rainfall and river flows in the continental US. *Geophysical*
759 *Research Letters, 28*(10), 2077–2080. https://doi.org/10.1029/2000GL012745

760 Ferguson, G., & St. George, S. (2003). Historical and estimated ground water levels near
761 Winnipeg, Canada, and their sensitivity to climatic variability. *Journal of the American*
762 *Water Resources Association, 39*(5), 1249–1259. Article. https://doi.org/10.1111/j.1752-
763 1688.2003.tb03706.x
764 Foster, T. E., & Brooks, J. R. (2001). Long-term trends in growth of *Pinus palustris* and *Pinus*
765 *elliottii* along a hydrological gradient in central Florida. *Canadian Journal of Forest*
766 *Research, 31*(10), 1661–1670. https://doi.org/10.1139/x01-100
767 Freund, M. B., Henley, B. J., Karoly, D. J., McGregor, H. V., Abram, N. J., & Dommenget, D.
768 (2019). Higher frequency of Central Pacific El Niño events in recent decades relative to
769 past centuries. *Nature Geoscience, 12*(6), 450–455. Article.
770 https://doi.org/10.1038/s41561-019-0353-3
771 Fritts, H. C. (1976). *Tree Rings and Climate*. New York: Academic Press.
772 Gholami, V., Torkaman, J., & Khaleghi, M. R. (2017). Dendrohydrogeology in
773 paleohydrogeologic studies. *Advances in Water Resources, 110*, 19–28. Article.
774 https://doi.org/10.1016/j.advwatres.2017.10.004
775 Gordu, F., & Nachabe, M. H. (2021). Hindcasting multidecadal predevelopment groundwater
776 levels in the Floridan aquifer. *Groundwater, 59*(4), 524–536. Article.
777 https://doi.org/10.1111/gwat.13073
778 Griffin, D., Meko, D. M., Touchan, R., Leavitt, S. W., & Woodhouse, C. A. (2011). Latewood
779 chronology development for summer-moisture reconstruction in the US Southwest. *Tree-*
780 *Ring Research, 67*(2), 87–101. https://doi.org/10.3959/2011-4.1
781 Harley, G. L., Maxwell, J. T., Larson, E., Grissino-Mayer, H. D., Henderson, J., & Huffman, J.
782 (2017). Suwannee River flow variability 1550–2005 CE reconstructed from a multispecies

783 tree-ring network. *Journal of Hydrology, 544*, 438–451.
784 http://dx.doi.org/10.1016/j.jhydrol.2016.11.020
785 Huang, B., Thorne, P. W., Banzon, V. F., Boyer, T., Chepurin, G., Lawrimore, J. H., et al. (2017).
786 Extended reconstructed sea surface temperature, version 5 (ERSSTv5): Upgrades,
787 validations, and intercomparisons. *Journal of Climate, 30*(20), 8179–8205.
788 https://doi.org/10.1175/jcli-d-16-0836.1
789 Huffman, J. M., & Rother, M. T. (2017). Dendrochronological field methods for fire history in
790 pine ecosystems of the Southeastern Coastal Plain. *Tree-Ring Research, 73*(1), 42–46.
791 https://doi.org/10.3959/1536-1098-73.1.42
792 Hunter, S. C., Allen, D. M., & Kohfeld, K. E. (2020). Comparing approaches for reconstructing
793 groundwater levels in the mountainous regions of interior British Columbia, Canada, using
794 tree ring widths. *Atmosphere, 11*(12), 25. Article. https://doi.org/10.3390/atmos11121374
795 Jasechko, S., & Perrone, D. (2021). Global groundwater wells at risk of running dry. *Science,*
796 *372*(6540), 418-+. Article. https://doi.org/10.1126/science.abc2755
797 Li, J. B., Xie, S. P., Cook, E. R., Morales, M. S., Christie, D. A., Johnson, N. C., et al. (2013). El
798 Niño modulations over the past seven centuries. *Nature Climate Change, 3*(9), 822–826.
799 Article. https://doi.org/10.1038/nclimate1936
800 Maleski, J. J., & Martinez, C. J. (2018). Coupled impacts of ENSO AMO and PDO on temperature
801 and precipitation in the Alabama–Coosa–Tallapoosa and Apalachicola–Chattahoochee–
802 Flint river basins. *International Journal of Climatology, 38*(S1), e717–e728.
803 https://doi.org/10.1002/joc.5401

804 Marella, R. L., & Berndt, M. P. (2005). *Water withdrawals and trends from the Floridan aquifer*
805 *system in the southeastern United States, 1950-2000*. Reston, Virginia: U.S. Geological
806 Survey Circular 1278.
807 McCabe, G. J., Betancourt, J. L., Gray, S. T., Palecki, M. A., & Hidalgo, H. G. (2008).
808 Associations of multi-decadal sea-surface temperature variability with US drought.
809 *Quaternary International, 188*, 31–40. Proceedings Paper.
810 https://doi.org/10.1016/j.quaint.2007.07.001
811 McCabe, G. J., Palecki, M. A., & Betancourt, J. L. (2004). Pacific and Atlantic Ocean influences
812 on multidecadal drought frequency in the United States. *Proceedings of the National*
813 *Academy of Sciences of the United States of America, 101*(12), 4136–4141.
814 https://doi.org/10.1073/pnas.0306738101
815 McCarroll, D., Young, G. H., & Loader, N. J. (2015). Measuring the skill of variance-scaled
816 climate reconstructions and a test for the capture of extremes. *The Holocene, 25*(4), 618–
817 626. https://doi.org/10.1177/0959683614565956
818 Meko, D. M. (1981). *Application of Box-Jenkins methods of time series analysis to the*
819 *reconstruction of drought from tree rings.* (Ph.D. Ph.D. Dissertation), University of
820 Arizona, Tucson, Arizona.
821 Miller, J. A. (1990). *Ground Water Atlas of the United States: Segment 6, Alabama, Florida,*
822 *Georgia, South Carolina* (730G). Retrieved from
823 http://pubs.er.usgs.gov/publication/ha730G
824 NCDC. (2018). Monthly Historical Climate Time Series. Retrieved from
825 https://www7.ncdc.noaa.gov/CDO/CDODivisionalSelect.jsp

826 Newman, M., Alexander, M. A., Ault, T. R., Cobb, K. M., Deser, C., Lorenzo, E. D., et al. (2016).
827 The Pacific Decadal Oscillation, revisited. *Journal of Climate, 29*(12), 4399–4427.
828 https://doi.org/10.1175/JCLI-D-15-0508.1
829 Outland III, R. B. (2004). *Tapping the Pines: The Naval Stores Industry in the American South*.
830 Baton Rouge, Lousiana: LSU Press.
831 Pederson, N., Bell, A. R., Knight, T. A., Leland, C., Malcomb, N., Anchukaitis, K. J., et al. (2012).
832 A long-term perspective on a modern drought in the American Southeast. *Environmental*
833 *Research Letters, 7*(1), 014034. https://doi.org/10.1088/1748-9326/7/1/014034
834 Perez-Valdivia, C., & Sauchyn, D. (2011). Tree-ring reconstruction of groundwater levels in
835 Alberta, Canada: Long term hydroclimatic variability. *Dendrochronologia, 29*(1), 41–47.
836 http://dx.doi.org/10.1016/j.dendro.2010.09.001
837 R Development Core Team. (2019). R: A language and environment for statistical computing
838 (Version v2.11.1). Vienna, Austria: R Foundation for Statistical Computing. Retrieved
839 from http://www.R-project.org
840 Schmidt, N., Lipp, E. K., Rose, J. B., & Luther, M. E. (2001). ENSO influences on seasonal rainfall
841 and river discharge in Florida. *Journal of Climate, 14*(4), 615–628.
842 https://doi.org/10.1175/1520-0442(2001)014<0615:EIOSRA>2.0.CO;2
843 SRWMD. (2020). Suwannee River Water Management District Groundwater Portal.
844 Stahle, D. W., Carr, D., Griffin, R. D., & Jennings, J. (2010). *NOAA/WDS Paleoclimatology -*
845 *Stahle - Upper Withlacoochee River - TADI - ITRDB FL009*. NOAA National Centers for
846 Environmental Information. https://doi.org/10.25921/gqph-x765. Accessed June 15, 2019.
847 Stahle, D. W., D'Arrigo, R., Krusic, P. J., Cleaveland, M. K., Cook, E., Allan, R. J., et al. (1998).
848 Experimental dendroclimatic reconstruction of the Southern Oscillation. *Bulletin of the*

American Meteorological Society, 79(10), 2137–2152. https://doi.org/10.1175/1520-0477(1998)079<2137:EDROTS>2.0.CO;2

Stahle, D. W., Fye, F. K., Cook, E. R., & Griffin, R. D. (2007). Tree-ring reconstructed megadroughts over North America since A.D. 1300. *Climatic Change, 83*(1), 133–149. journal article. https://doi.org/10.1007/s10584-006-9171-x

Sutton, C., Kumar, S., Lee, M. K., & Davis, E. (2021). Human imprint of water withdrawals in the wet environment: A case study of declining groundwater in Georgia, USA. *Journal of Hydrology-Regional Studies, 35*, 16. Article. https://doi.org/10.1016/j.ejrh.2021.100813

Tegel, W., Seim, A., Skiadaresis, G., Ljungqvist, F., Kahle, H.-P., & Land, A. (2020). Higher groundwater levels in western Europe characterize warm periods in the Common Era. *Scientific Reports, 10*. https://doi.org/10.1038/s41598-020-73383-8

Tootle, G. A., & Piechota, T. C. (2006). Relationships between Pacific and Atlantic ocean sea surface temperatures and U.S. streamflow variability. *Water Resources Research, 42*(7), W07411. https://doi.org/10.1029/2005wr004184

Torbenson, M. C. A., Stahle, D. W., Howard, I. M., Burnette, D. J., Villanueva-Diaz, J., Cook, E. R., & Griffin, D. (2019). Multidecadal modulation of the ENSO teleconnection to precipitation and tree growth over subtropical North America. *Paleoceanography and Paleoclimatology, 34*(5), 886–900. Article. https://doi.org/10.1029/2018pa003510

Torrence, C., & Compo, G. P. (1998). A practical guide to wavelet analysis. *Bulletin of the American Meteorological Society, 79*(1), 61–78. https://doi.org/10.1175/1520-0477(1998)079<0061:APGTWA>2.0.CO;2

Trouet, V., & Van Oldenborgh, G. J. (2013). KNMI Climate Explorer: A web-based research tool for high-resolution paleoclimatology. *Tree-Ring Research, 69*(1), 3–13. https://doi.org/10.3959/1536-1098-69.1.3

Vines, M., Tootle, G., Terry, L., Elliott, E., Corbin, J., Harley, G. L., et al. (2021). A paleo perspective of Alabama and Florida (USA) interstate streamflow. *Water, 13*(5), 657–668. https://doi.org/10.3390/w13050657

Volk, M. I., Hoctor, T. S., Nettles, B. B., Hilsenbeck, R., Putz, F. E., & Oetting, J. (2017). Florida Land Use and Land Cover Change in the Past 100 Years. In E. P. Chassignet, J. W. Jones, V. Misra, & J. Obeysekera (Eds.), *Florida's climate: Changes, variations, & impacts* (pp. 51–82). Gainesville, Florida: Florida Climate Institute.

Wigley, T. M. L., Briffa, K. R., & Jones, P. D. (1984). On the average value of correlated time series, with applications in dendroclimatology and hydrometeorology. *Journal of Climate and Applied Meteorology, 23*(2), 201–213. https://doi.org/10.1175/1520-0450(1984)023<0201:OTAVOC>2.0.CO;2

Wise, E. K., & Dannenberg, M. P. (2019). Climate factors leading to asymmetric extreme capture in the tree-ring record. *Geophysical Research Letters, 46*(6), 3408–3416. https://doi.org/10.1029/2019gl082295

Yeh, S. W., & Kirtman, B. P. (2005). Pacific decadal variability and decadal ENSO amplitude modulation. *Geophysical Research Letters, 32*(5). https://doi.org/10.1029/2004GL021731

Zang, C., & Biondi, F. (2015). treeclim: an R package for the numerical calibration of proxy-climate relationships. *Ecography, 38*(4), 431–436. https://doi.org/10.1111/ecog.01335